Global and Planetary Change 249 (2025) 104778

Contents lists available at ScienceDirect

Global and Planetary Change

journal homepage: www.elsevier.com/locate/gloplacha

Undervalued CO_2 emissions from soil to the atmosphere in seismic areas: A case study in Tangshan, North China

Le Hu [a,b], Ying Li [a,b,*], Zhaofei Liu [a,b], Chang Lu [a,b], Giovanni Martinelli [c], Galip Yuce [d], Jianguo Du [a,b]

[a] Institute of Earthquake Forecasting, China Earthquake Administration, Beijing, China
[b] Key Laboratory of Earthquake Forecasting and Risk Assessment, Ministry of Emergency Management Beijing, China
[c] INGV-National Institute of Geophysics and Volcanology Dept. of Palermo, Palermo, Italy
[d] Department of Geological Engineering, Hacettepe University, Ankara, Turkey

ARTICLE INFO

Editor Name: Prof. Liviu Matenco

Keywords:
Soil CO_2 emission
Seismicity
Annual CO_2 flux
The Tangshan region

ABSTRACT

A large quantity of CO_2 produced in the Earth's interior is emitted to the atmosphere via soil diffusion, especially in active tectonic areas. Due to the lack of extensive in situ measurements, however, estimations of soil CO_2 output have been poorly constrained thus far, leading to the perception that soil CO_2 seems to be a marginal source of global carbon emissions. Here, the contribution of soil CO_2 to the atmosphere is discussed based on soil degassing rates measured at 187 sites in the Tangshan seismic area, North China. The measured degassing rates ranged from 9.04 g $m^{-2}d^{-1}$ to 230.42 g·$m^{-2}d^{-1}$, with an average of 87.46 g·$m^{-2}d^{-1}$, suggesting that high degassing rates are common throughout the region. Carbon isotopic results show that the soil CO_2 comes mainly from the deep-seated carbonates and shallow biogenetic processes. Using the threshold value of the data population (96.20 g·$m^{-2}d^{-1}$), the background and anomalous areas are distinguished. We find that anomalous degassing areas overlap well with epicenters of earthquakes with magnitudes greater than 5. The total annual CO_2 output in anomalous areas was estimated to be 38 Mt. This extremely high value can be attributed to the enlarged degassing areas and enhanced CO_2 emissions induced by regional active faults and frequent seismic activities. Our results indicate that the impact of soil CO_2 emissions in seismic regions should receive increased attention.

1. Introduction

Global climate change has become an important theme and has captured the attention of worldwide multidisciplinary scientific communities. Carbon dioxide (CO_2), as one of the most important greenhouse gases, affects the temperature of the Earth's atmosphere and plays an important role in the climate (e.g., Brune et al., 2017; Farsang et al., 2021; Mason et al., 2017). Terrestrial CO_2 emissions, which account for a substantial quantity of the global carbon budget, have drawn widespread attention in recent years (e.g., Bornemann et al., 2022; Buttitta et al., 2023; Caracausi and Sulli, 2019; Foley and Fischer, 2017; Lee et al., 2016; Tamburello et al., 2018). Earth's degassing of CO_2 occurs persistently during geological evolution, especially in active volcanic and tectonically active areas (e.g., Brune et al., 2017; Foley and Fischer, 2017; Tamburello et al., 2018). For a long time, volcanoes have been regarded as the most important chimneys of CO_2 emissions on Earth; thus, their contributions to the atmosphere have been intensely investigated (e.g., Burton et al., 2013; Lopez et al., 2023). However, even in volcanic areas, the CO_2 flux via soil diffusion can reach nearly one-third of the total output (Burton et al., 2013). Within this context, invisible CO_2 seepage to the atmosphere from soils should be a competitive CO_2 supplier for the global budget. On the other hand, although volcanic conduits provide channels for CO_2 transport, their number worldwide is limited; therefore, the CO_2 released from other more widely distributed geological structures cannot be ignored (Brune et al., 2017; Camarda et al., 2019; Girault et al., 2018; Lee et al., 2016; Mörner and Etiope, 2002).

Active faults, which are defined as faults that have recently experienced dynamic movements, are extensively distributed on the Earth's surface. These faults provide numerous pathways for the migration of deep-sourced gases that are emitted from the crust to the atmosphere because these regions have increased permeability and porosity (e.g.,

* Corresponding author.
E-mail address: liying@ief.ac.cn (Y. Li).

https://doi.org/10.1016/j.gloplacha.2025.104778
Received 15 July 2024; Received in revised form 28 February 2025; Accepted 28 February 2025
Available online 2 March 2025

Caracausi et al., 2023; Chiarabba et al., 2022; Chiodini et al., 2010). Soil CO_2 fluxes along faults in active volcanic and/or geothermal areas have frequently been reported (e.g. Chiodini et al., 2004; Kis et al., 2017). In addition, along some large-scale faults – such as the San Andreas Fault – cross-fault CO_2 flux measurements have also been conducted to assess the fault activity (e.g., Lewicki and Brantley, 2000). However, beyond these areas, the contribution of soil CO_2 to the atmosphere is not understood well due to the absence of systematic in situ measurements and quantitative evaluations. This is likely because there are countless active faults worldwide that have different initial activity ages. In addition, certain pre-existing inactive faults can become reactivated due to dynamic changes (e.g., Hencz et al., 2023). Therefore, it is difficult to ascertain whether some so-called active faults are still active at present, as a result of which it is difficult to assess their actual degassing potentials. Seismicity is an apparent indicator that faults are very active. Many studies have shown that the outgassing of CO_2 can be pumped by earthquakes because they dynamically affect crust permeability (e.g., Chiodini et al., 2020; Girault et al., 2018; Ingebritsen et al., 2016). Given that it is still difficult to investigate soil CO_2 degassing rates at all active faults worldwide, considering the most recently active faults in seismic areas as research objects can make it feasible to obtain credible data to assess whether such emissions should be focused on when considering the present-day CO_2 atmospheric budget. Therefore, in the present study, in the classical Tangshan seismic area of northern China, where the Tangshan M_S 7.8 earthquake occurred on 28 July 1976, followed by hundreds of aftershocks, the soil CO_2 degassing characteristics were investigated, and the total CO_2 output was assessed.

2. Seismotectonic setting

The Tangshan region is located in the northern part of China, and tectonically, it belongs to the rift-depression basin of North China (Fig. 1a). Controlled by far-field tectonic forces owing to the northeastward compression of the Tibetan Plateau and the westward subduction of the Pacific Plate (Li et al., 2016), the area is the most active (Fig. 1b) and earthquake prone areas in North China (Liu et al., 2020). Due to a prolonged period of thermal subsidence since the early Tertiary (Allen et al., 1997), most of the research area was covered by fine to coarse sandy sediments with the largest thickness exceeding 2 km. Pre-Cenozoic rocks can be found sporadically in the northern part of the study area (Fig. 1c), which is composed mainly of Precambrian metamorphic basement rocks, metasandstones and carbonates; Cambrian–Ordovician limestone, dolomitic limestone, and argillaceous limestone; and middle Carboniferous–Permian sandstone, siltstone, and mudstone, with multilayer coal seams. A high-precision deep seismic reflection profile (Fig. 1c) has outlined the rough underground stratigraphic boundaries (as shown in Fig. 8, Liu et al., 2011). According to the results, the depth of Ordovician strata is about 4–6 km and the depth of crystalline basement is about 8–10 km. Thus, carbonate rock is abundant underground as it dominates the rock types in this depth interval.

Regional faults are well developed in the Tangshan region. Four faults with ENE and NNW trends confine the city area of Tangshan into a rhombic block (Fig. 1c). The Tangshan fault zone, traversing the block, comprises three active faults, from south to north: the Tangshan-Guye fault (F_1), Weishan-Changshan fault (F_2), and Douhe fault (F_3). All of these faults are NE-trending (25–35°) normal faults with dextral strike-slip components and NW dip angles ranging from 70° to 80° (Liu et al., 2011). The Tangshan fault zone is considered a complex fault system that developed from the deep crust to the shallow crust (Liu et al., 2022; Zhang et al., 2022). The 1976 Tangshan M_S 7.8 earthquake struck the Tangshan fault zone, causing a 10 km-long rupture zone (Liu et al., 2022). This earthquake caused more than 240,000 fatalities and considerable economic loss and was one of the most destructive natural disasters in the modern world (Cai et al., 2023). Afterward, long-lasting aftershocks occurred countless times. At present, at least one $M_S \geq 3.0$

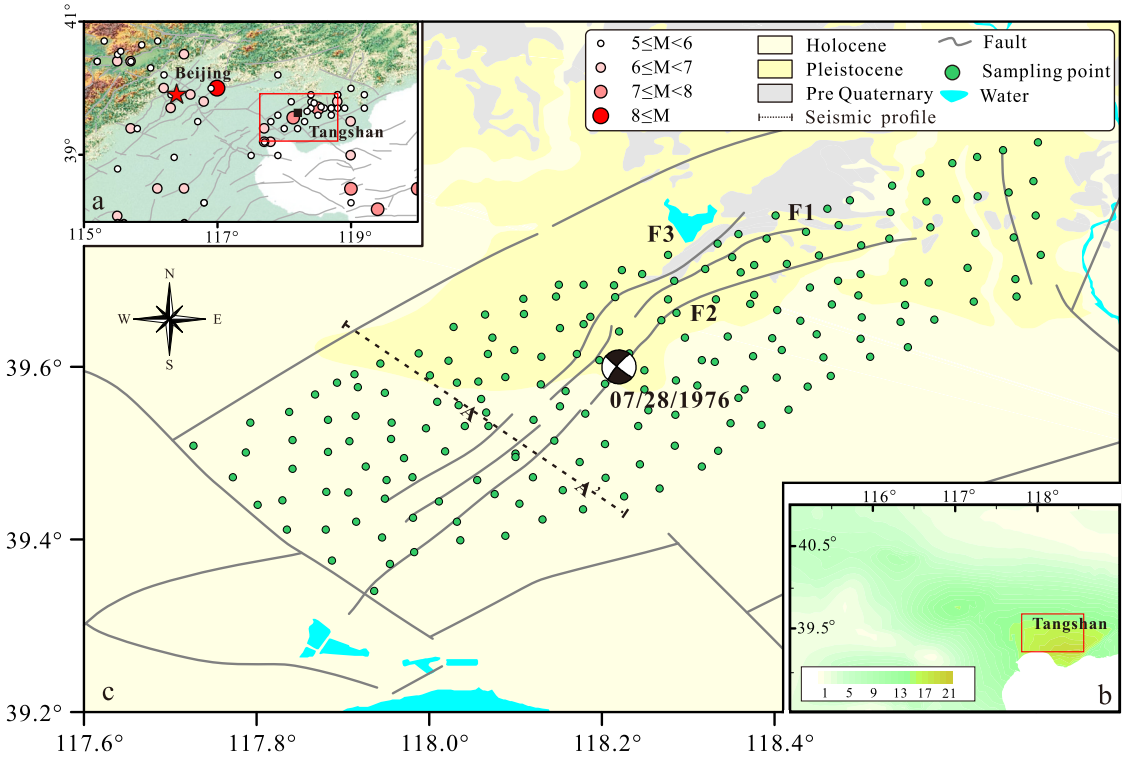

Fig. 1. (a) Regional setting and location of the study area (red box). (b) Shear rate distribution on the study region and adjacent areas. The data are obtained from Wang and Shen (2020). (c) Geological map of the study region (modified from Liu et al., 2022) and the distribution of measurement sites. The location of the seismic reflection profile is according to Liu et al. (2011). A-A' represent the profile range adopted in Fig. 8. (For interpretation of the references to colour in this figure legend, the reader is referred to the web version of this article.)

earthquake occurs once every two years.

3. Methods

An extensive soil gas CO_2 flux survey was conducted throughout the Tangshan region, covering the three active faults of the Tangshan fault zone. In total, 187 field points (Fig. 1) were measured within 20 days in August 2021 during which the weather remained clear and the surface meteorological factors were mostly consistent. We conducted the measurements from 9:30 to 16:00 each day to minimize the difference in the biological activity. When sampling, a hemispherical chamber with a radius of 0.2 m was used and connected to the inlet and outlet of the gas detector through rubber tubes (Fig. 2). An inlet filter and desiccant were used to protect the detector from dust and soil moisture (>10 %). The CO_2 was pumped continuously for 30 min by a GXH-3010E portable infrared CO_2 analyzer at a sampling interval of 15 s. The soil temperature, air temperature and atmospheric pressure were also recorded at each measurement point.

The calculation of soil gas CO_2 flux ($FluxCO_2$) was performed using the following equation (Chiodini et al., 1998, 2010):

$$Flux_{CO2} = \frac{\Delta c}{A_c \Delta t} = \frac{\rho_{std} \times V_{std}}{A_c} \bullet \frac{dc}{dt} = \frac{\rho_{std}}{A_c} \bullet \frac{V_c P_c T_{std}}{P_{std} T_c} \bullet \frac{dc}{dt}$$

where ρstd represents the density of CO_2 at normal pressure and temperature (1.977 $kg \cdot m^{-3}$); Δc represents the CO_2 concentration ($Bq \cdot m^{-3}$) variations with time in the chamber during the measuring period Δt (min); Pstd and Tstd represent the standard barometric pressure (101.325 kPa) and temperature (273.15 K) respectively; V_C represents the volume of the chamber (m^3); A_C represents the surface area of the chamber base (m^2); P_C represents the atmospheric pressure (Pa); T_C represents the measured soil temperature (K); and dc/dt represents the rate of CO_2 concentration increase in the chamber.

Three soil gas samples were collected using conventional water displacement methods for carbon isotope analysis, the detailed analytical methodology is presented in (Liu et al., 2024). The $\delta^{13}C_{CO2}$ values were analyzed at the Lanzhou Center for Oil and Gas Resources, Chinese Academy of Sciences, using an Agilent 6890 gas chromatograph coupled to Thermo Fisher Scientific Delta Plus-XP stable. The $\delta^{13}C$-$_{CO2}$ values were expressed using traditional delta numeration, with a measurement error of ±0.2 ‰ per milliliter (‰) against the reference standard of Pee Dee Belemnite (PDB).

4. Results

The obtained CO_2 fluxes ranged from 9.04 $g \cdot m^{-2} d^{-1}$ to 230.42 $g \cdot m^{-2} d^{-1}$, with a mean value of 87.46 $g \cdot m^{-2} d^{-1}$ (Appendix 1 and Table 1). The soil temperature, air temperature (Fig. 3) and atmospheric pressure (within a very narrow range) are analyzed and their effects on the flux values are excluded. Considering the large variability in the flux values, statistical methods can be used to calculate the threshold values of anomalies. The quantile–quantile plot (Q–Q plot) is a widely used method for estimating the threshold of a dataset (e.g., Ciotoli et al., 2014; Fu et al., 2017; Yuce et al., 2017); the data under and above the threshold represent background and anomalous value populations, respectively. As shown in Fig. 4, where the horizontal axis represents the actual measured values and the vertical axis represents the theoretical values based on the normal distribution, the CO_2 flux data were distributed along two straight lines with different slopes. The abscissa value of the intersection of the two lines, which is also the inflection point of the dataset, is 96.20 $g \cdot m^{-2} d^{-1}$, which is the threshold value of the anomalous CO_2 fluxes.

The $\delta^{13}C$-$_{CO2}$ values of the samples exhibit a narrow range, from −18.8 to −19.9 (Table 2). This result is similar to the data obtained in previous research (Chen et al., 2019). However, it is important to note that these $\delta^{13}C$-$_{CO2}$ values are obtained from samples collected in summer, when the biological activity is relatively intense.

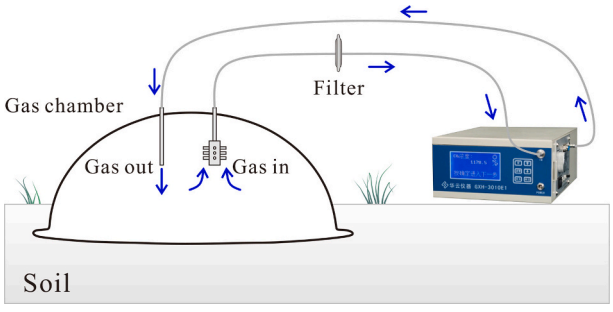

Fig. 2. Schematic diagram of soil gas CO_2 flux measurement.

5. Discussion

5.1. Origins of the soil CO_2

Generally, soil CO_2 is primarily generated by organic matter decomposition and microbial and root respiration during biological processes. According to previous studies on various ecosystems (Raich and Schlesinger, 1992; Raich and Tufekcioglu, 2000), the organic soil CO_2 flux can reach 21 $g \cdot m^{-2} d^{-1}$. However, in tectonically active areas, the soil CO_2 flux can exceed this value via deep supply through highly permeable areas like faults and associated fissures (Chiodini et al., 2010, 2020; Chiarabba et al., 2022; Caracausi et al., 2023). In this study, the mean flux (87.46 $g \cdot m^{-2} d^{-1}$) far exceeds this value and is much greater than the reported global average soil flux based on extrapolations from biome land areas (4.90 $g \cdot m^{-2} d^{-1}$, Raich and Schlesinger, 1992) and the highest value (63.00 $g \cdot m^{-2} d^{-1}$ Lewicki and Brantley, 2000) measured in the San Andreas Faults in the United States, indicating the excess geological CO_2 supplies.

Unlike volcanic or geothermal areas, which have abundant CO_2 supplies from underground magmas and thus extremely high deeply-derived CO_2 fluxes are frequently detected (Parks et al., 2013; Cardellini et al., 2017), the Tangshan region is underlined by thick sediments where no fumaroles or thermal springs occur; additionally, soil diffusion is the only way for CO_2 emissions to increase. In fact, it is difficult to accurately determine the origins of CO_2 by simply using the $\delta^{13}C$ values, as there are some overlaps in carbon isotopic compositions from different sources. In some cases, when combined with helium isotopes, the quantities of deeply-derived CO_2 can be inferred (Sano and Wakita, 1985). However, in the Tangshan region, deeply-derived ^3He cannot be determined accurately (Chen et al., 2019) owing to the 'atmospheric imprint'. Thus, it is not suitable to use the carbon and helium isotopes to determine the involvement of the deep-seated CO_2. However, in the graph of $\delta^{13}C$ vs. the CO_2 concentration (Fig. 5), it can still be found that soil CO_2 in the Tangshan region comes from the mixing of the deeply-derived CO_2 and biogenic CO_2, though the proportions cannot be determined due to large value spans of each source. Deeply-derived CO_2 usually includes CO_2 generated by mantle degassing, magmatic activity and/or decarbonation of carbonate rocks. The former two show $\delta^{13}C$ values of −4 to −8 (Sano and Wakita, 1985; Macpherson and Mattey, 1994); the latter one, according to the analytical results of carbonate rocks in the Tangshan region, ranges from −7.11 to 0.76 (Yang et al., 2013). Degassed CO_2 from the lithospheric mantle, even in the presence of deep-cutting faults, would be minor when reaching the earth's surface after long-distance migration (e.g. Wang et al., 2023). In addition, the lack of current subsurface magmatism in the area makes the magmatic origin of CO_2 in the region unlikely. Therefore, the abundant carbonate rocks, as mentioned earlier, should be the major source for the deeply-derived CO_2 in the region. In conclusion, the soil CO_2 in the Tangshan region is generated mainly by the decomposition of organic matter (biogenic source) and the decarbonation of carbonate rocks. The

Table 1
Statistics of the soil gas flux and environmental parameters measured in the Tangshan region.

	Min	Max	Mean	Median	Lower Quartile	Upper Quartile
Altitude (m/sea level)	−23.14	73.90	19.35	14.30	3.70	32.88
Atmospheric pressure (Pa)	99,812	101,626	100,831	100,928	100,460	101,152
Air temperature (°C)	24.0	37.8	30.4	30.1	28.6	32.2
Soil temperature (°C)	22.1	33.8	27.1	26.8	25.5	28.4
CO_2 flux ($g{\cdot}m^{-2}d^{-1}$)	9.04	230.42	87.46	81.31	56.32	108.69

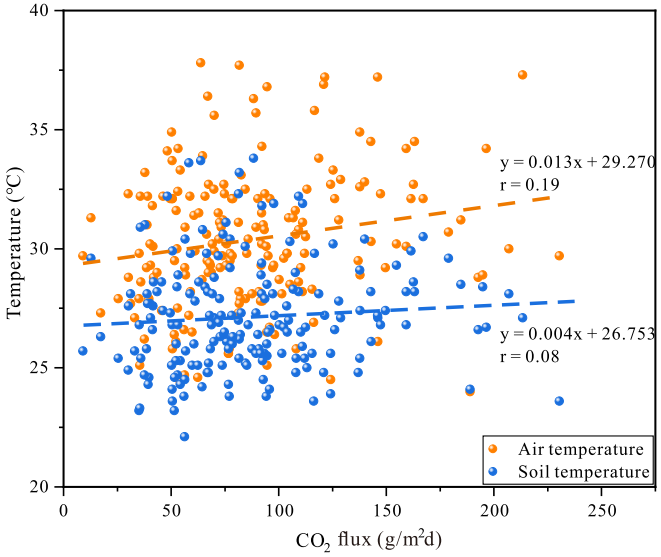

Fig. 3. CO_2 flux vs. air temperatures and soil temperatures. The red and blue dashed lines are Pearson correlation fitting lines, and r represents the correlation coefficient. (For interpretation of the references to colour in this figure legend, the reader is referred to the web version of this article.)

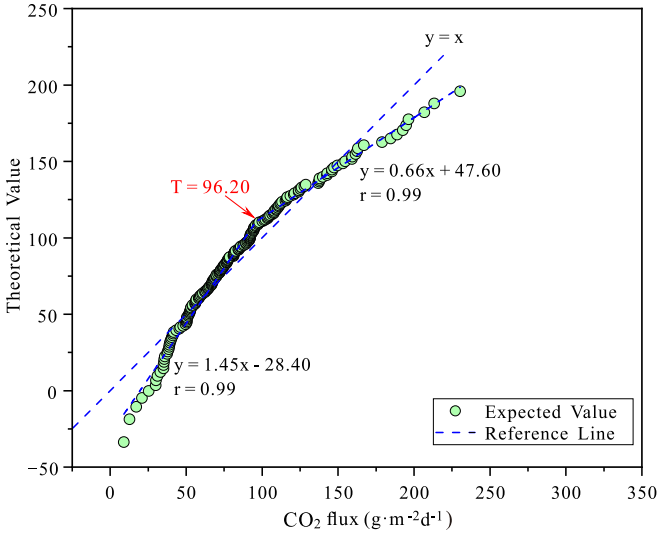

Fig. 4. Quantile–quantile plots of calculated soil CO_2 fluxes indicating that the soil gas data are separated into two different populations recognizable by the inflection point on the curve. The horizontal axis and vertical axis represent the measured value and the theoretical values based on a normal distribution, respectively.

biogenic source is probably Carboniferous-Permian coal seams and Cenozoic organic material-bearing sediments, while the carbonate-derived CO_2 is generated mainly from the carbonate strata deposited during geological time.

5.2. Spatial variation and its controlling factors

According to previous research, the soil gas degassing rate is closely related to the distance from the fault: it usually reaches its highest value in or near the fault core, and then decays rapidly (Ciotoli et al., 2005; Bond et al., 2017). This phenomenon also occurs on many active fault zones in north China (Wang et al., 2017). This is because the fault cores are characterized by high permeability, which is a key factor influencing gas emissions (Fu et al., 2017; Yuce et al., 2017; Chiarabba et al., 2022; Caracausi et al., 2023). However, in the Tangshan region, based on the measured average data, most of the area exhibits high degassing rates, indicating that the permeability of rocks and soils is significantly elevated, which is probably caused by crustal movements, as evidenced by the frequent seismic events and high shear rates in the region (Fig. 1 b, c).

Using the kriging interpolation method, a contour map of the CO_2 flux in the Tangshan region was constructed, where anomalous and background areas were distinguished using the threshold value (96.20 $g{\cdot}m^{-2}d^{-1}$) as the boundary of the colour bar (Fig. 6). Because this study was designed and conducted in a localized area, the background rock types and soil compositions at each measurement point can be considered consistent. Thus, the permeability of rocks and soils is the governing factor controlling regional CO_2 emissions. Conventionally, active faults are considered gas migration pathways due to their enhanced permeability. However, as shown in Fig. 6, the anomalous areas of CO_2 flux are not entirely concordant with the surface traces of faults in the area. This could be partly caused by the complex structure of the Tangshan fault zone. The results of deep seismic reflection profiles across the area indicate that the fault systems are characterized by typically positive flower structures comprising multiple branch faults in the upper crust and an upright strike-slip main fault cutting the lower crust (Liu et al., 2011). These branch faults all converge downward to the main faults and exhibit different occurrences, activities and features due to the stress field during different geological periods. In addition, some branch faults have their own branches distributed in the Cenozoic sedimentary layers, as revealed by shallow seismic and drilling explorations (Liu et al., 2022). Therefore, beyond the faults that have been previously mapped out (Fig. 1c), other high-permeability areas for underground gas migration could also exist.

In addition to the movement of active faults, the permeability within a local region is also affected by earthquakes, which can damage rocks, create new pathways, and connect deep rocks to the Earth's surface (Chiodini et al., 2020; Girault et al., 2018; Ingebritsen et al., 2016). In Fig. 6, the rupture zone of the Tangshan M_S 7.8 earthquake is marked by a high CO_2 flux distribution. This implies that CO_2 degassing through newly damaged zones resulting from recent earthquakes can be more efficient than degassing through pre-existing active faults. Thus, the occurrence of earthquakes in the region probably had an important influence on the emission of CO_2. To investigate this, earthquake data starting from the Tangshan M_S 7.8 earthquake were extracted from the catalogue (https://data.earthquake.cn/), and magnitudes greater than 2, 3, 4 and 5 were distinguished for plotting on the contour map of the CO_2 flux. It can be seen that earthquakes with magnitudes greater than 2

Table 2
Carbon isotope ratio values of soil gas CO_2 in the Tangshan region. L1 ~ L9 refers to data from literature (Chen et al., 2019).

	S1	S2	S3	L1	L2	L3	L4	L5	L6
CO_2 concentrations (%)	4.02	2.05	10.78	8.96	11.24	2.42	6.76	2.46	3.27
δ13C-$_{CO2}$	−19.3	−18.8	−19.9	−18.4	−19.7	−17.3	−19.8	−18.2	−20.6

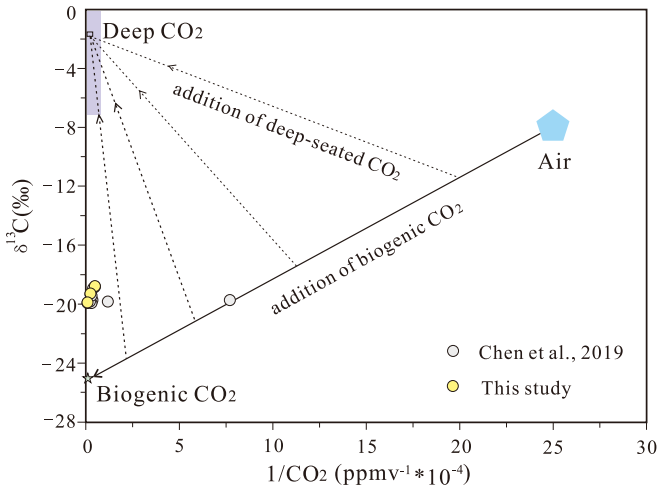

Fig. 5. $\delta^{13}C_{-CO2}$ vs. CO_2 concentration plot of the analyzed gas samples (modified from Parks et al., 2013).

and 3 cover both background and anomalous areas, and exhibit no correlations with CO_2 flux distributions (Fig. 7a, b). However, as the magnitude increases to 4, the epicenters become prominently concentrated in the anomalous areas (Fig. 7c), and when the magnitude reaches 5, the epicenters of earthquakes overlap well with the areas where anomalous CO_2 fluxes are distributed (Fig. 7d). The occurrence of an earthquake involves a process of energy transmission and consumption. As most earthquakes have occurred within the middle crustal depth in the Tangshan region, the energy generated by earthquakes can easily be transferred to the overlying strata. According to the empirical equation '$\mathrm{Log}E = 11.8 + 1.5\,M$' between magnitude ($M$) and energy ($E$) proposed by Gutenberg and Richter (1956), a magnitude 5 earthquake can produce almost 1000 times more energy than a magnitude 3 earthquake. Further, large earthquakes can produce enough energy to damage overlying rocks and enhance vertical permeability, even to the near-surface; this phenomenon has also been indicated by the regional 3-D velocity model, which exhibits a decrease in Vp values from the shallow to the deep crust (Zhang et al., 2022). Relatively small earthquakes, which create less energy, affect only limited areas around the epicentre but can still facilitate gas emission through the passage of seismic waves (Gresse et al., 2016).

Tomographic results revealed significant velocity anomalies in the lower crust, which were interpreted as the result of the underplating of mantle magma (Liu et al., 2011; Zhang et al., 2022). If this process actually occurs, even in the absence of any Cenozoic volcanism in the Tangshan region, such hot melt and its derived fluids could help extract CO_2 from the overlying rocks by heating and through fluid–rock interaction processes, as the case occurred in many volcanic areas such as Santorini, Greece (Parks et al., 2013) and Campi Flegrei, Italy (Buono et al., 2023). In addition, earthquakes can directly facilitate thermal decarbonation in carbonate layers triggered by frictional heating due to relative sliding between two sides of a fault (Italiano et al., 2015; Violay et al., 2013). Therefore, in the study area, frequent earthquakes can help both produce CO_2 and generate pathways for CO_2 migration. The anomalous fluxes are likely to have more carbonate-derived CO_2 supplies (Fig. 8).

5.3. Total annual CO_2 emission

CO_2 entering the atmosphere, regardless of its origin, generates a 'greenhouse effect' (e.g., Schneider, 1989; Anderson et al., 2016). Since the anomalous CO_2 flux areas and the background areas can be distinguished from each other (Fig. 6), the squared paper method was applied for the calculation in the area. Then, using the average values of the anomalous populations (135.72 $g{\cdot}m^{-2}d^{-1}$) and the area (775 km^2), the total annual anomalous CO_2 output was found to be 38 $Mt.{\cdot}yr^{-1}$. However, consistent with the defects in previous studies, it should be noted that this annual value is a rough estimate, as seasonal factors were not considered.

Fig. 9 shows the comparison of the annual total CO_2 output in the study area with that in other active volcano-geothermal or tectonic regions at different scales. The CO_2 output in the study area is greater than the total amount of CO_2 generated from volcano-geothermal regions in China, comparable to that from geothermal systems along the Pacific rim, and accounts for nearly 7 % of the global subaerial volcanic CO_2

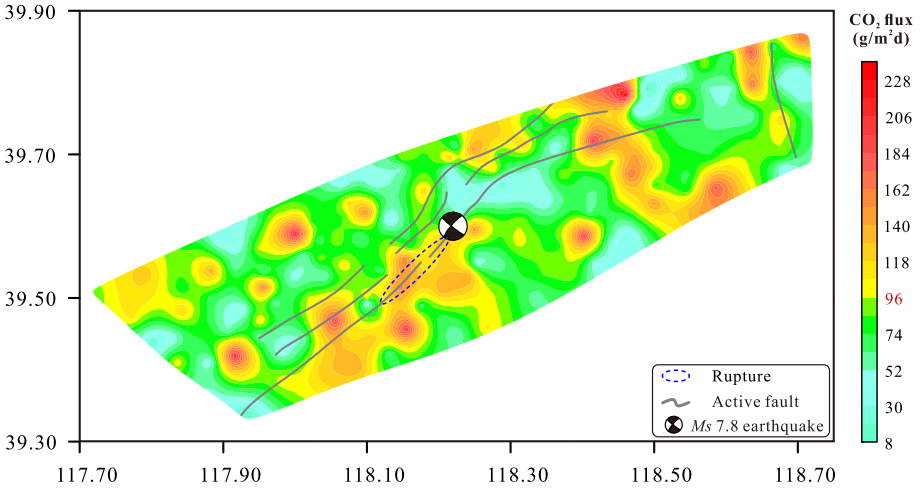

Fig. 6. Contour map of soil CO_2 fluxes in the study area.

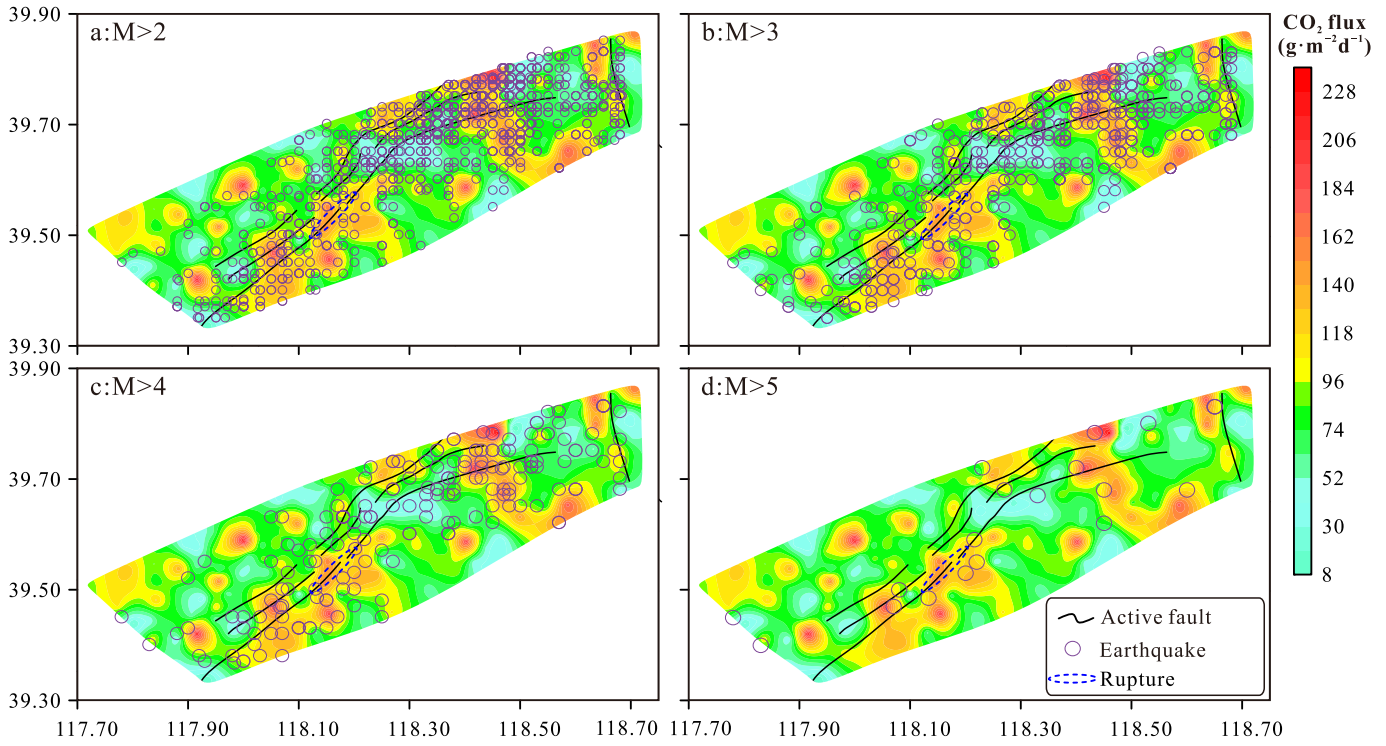

Fig. 7. Spatial distribution of earthquakes according to magnitude categories >2 (a), >3 (b), >4 (c), >5 (d), respectively, recorded in the study region since 1976 on the background of the measured soil CO_2 fluxes. Earthquake data are from China Earthquake Networks Center (http://www.cenc.ac.cn).

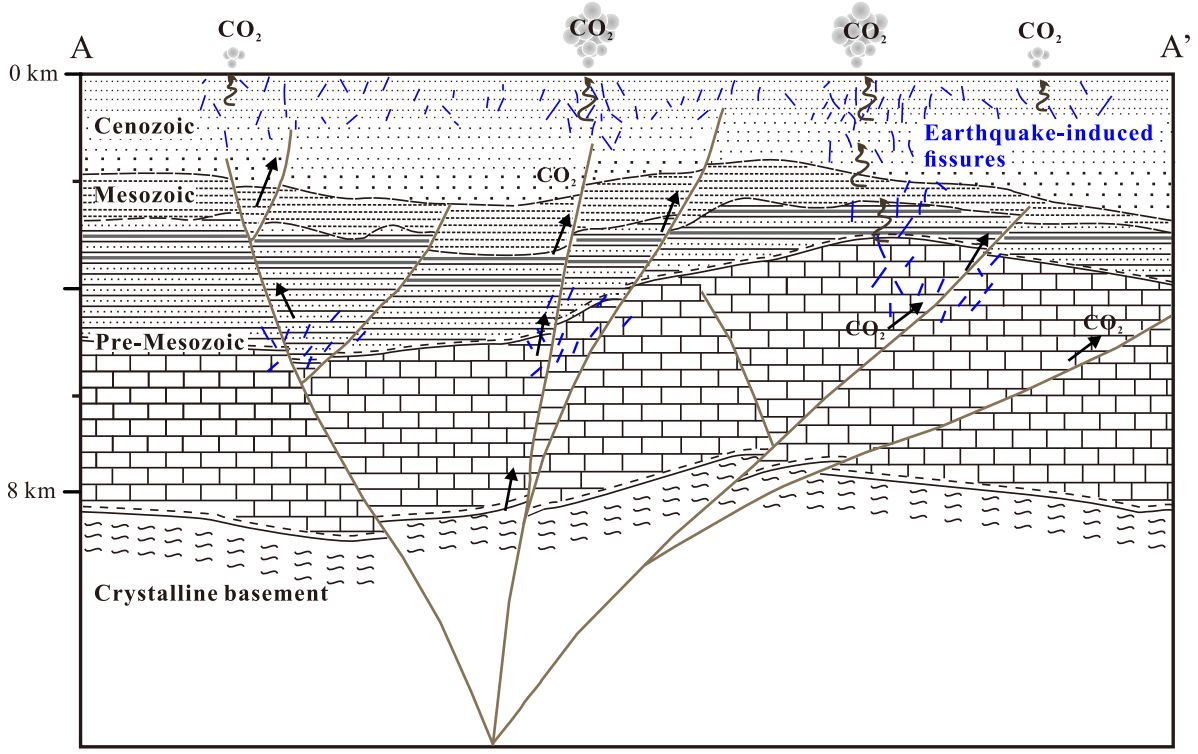

Fig. 8. Generic two-dimensional sketch showing CO_2 migration via both faults and earthquake-induced pathways. Fault configuration and strata boundaries according to interpretation of seismic reflection profiles (Liu et al., 2011).

flux. Although these values are probably underestimated because they originate from extrapolations based on small numbers of direct measurements, there is no doubt that a considerable amount of CO_2 is emitted to the atmosphere from the study region.

Soil diffusion is an important pathway for terrestrial CO_2 emissions (Camarda et al., 2019 and reference therein). Although the emission rate of CO_2 via soil diffusion may be lower than that via volcanic conduits, the total soil CO_2 output can be significant due to the large areal extent

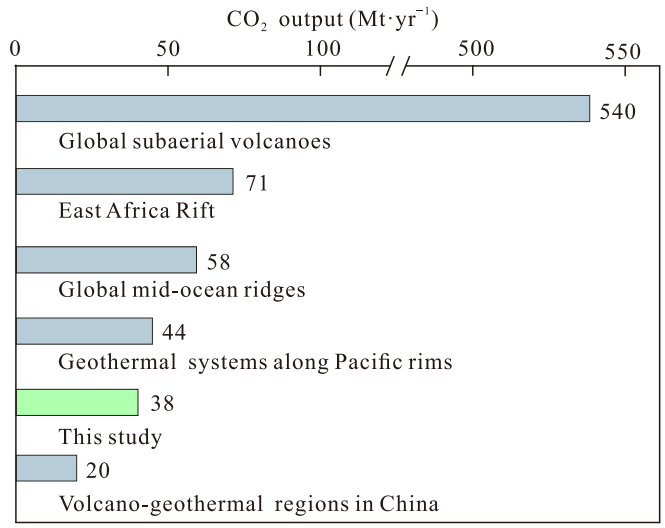

Fig. 9. Comparison of the annual CO_2 output range of the study region with those of volcanic or geothermal regions worldwide. The data for global subaerial volcanoes, global mid-ocean ridges, the East African Rift, geothermal systems along Pacific rims, and volcano-geothermal regions in China are from Burton et al. (2013), Le Voyer et al. (2019), Lee et al. (2016), Seward and Kerrick (1996), and Zhao et al. (2018), respectively.

(Burton et al., 2013). For this reason, even in volcanic regions, the soil CO_2 flux accounts for a significant proportion of the total output. CO_2 emissions to the atmosphere, regardless of the form, are controlled mainly by sources and emission channels. Globally, high-CO_2 emission areas are distributed around active continental margins (Tamburello et al., 2018), where deep-cutting faults and frequent seismic activity occurs; the magmatic degassing and metamorphism of marine sediments can produce significant amounts of CO_2. Locally, as found in this study, enhanced emissions can be attributed to regional active faults, continuous seismic activity, and abundant CO_2-bearing rocks.

Crustal carbonates are one of the most important sources of global carbon (Mason et al., 2017). Numerous studies have focused on the recycling process of these compounds during subduction (Mason et al., 2017; Plank and Manning, 2019). However, it has been estimated that the subducted crustal carbon flux into the mantle exceeds the flux emitted by volcanoes by an order of magnitude (Hazen and Schiffries, 2013). This implies that deep-stored carbon is relatively difficult to transport to the earth's surface and emit into the atmosphere. In contrast, crustal carbon is more easily affected by variations in stress and release to the atmosphere due to a shorter path of migration. The Tibetan Plateau is one of the most tectonically active places in the world and is characterized by intense crust–mantle interactions; for example, degassing CO_2 from most thermal springs or soils along active faults has been proven to originate mainly from the crust (Wang et al., 2023; Zhang et al., 2021). Thus, awareness should be raised that crustal carbonate and carbonate-bearing rocks deposited at different geological times can also act as direct sources of CO_2 (Parks et al., 2013; Violay et al., 2013; Buono et al., 2023).

Carbonate strata are widely distributed worldwide. If the CO_2 generated by the metamorphism of carbonates in active tectonic structures is released into the atmosphere, as has occurred in the Tangshan region, an unexpectedly high flux can occur. Nevertheless, quantifying this value is difficult because many degassing sites are present throughout the world, and extensive in situ measurements are seldom performed (Burton et al., 2013). Additionally, extrapolation cannot be used due to differences in the geological background, fault activity and earthquake occurrence at each site. Therefore, a more detailed regional division in combination with CO_2 emission mapping of typical regions is required in future research. However, based on the CO_2 outputs calculated at a local scale in this study, we suggest that the total amount of CO_2 emissions, at least in seismic areas, is highly underestimated and needs to be reconsidered.

6. Conclusions

In this study, we conducted high-density measurements of the soil CO_2 degassing rate in the whole Tangshan seismic region. Our results show that the high-flux area does not completely coincide with the trajectory of the fault lines on the surface, suggesting that the high-permeability areas in active fault zones are not distributed only around the traces of faults on the surface. Due to the structural complexity of faults from deep to shallow, the morphological characteristics of faults should also be considered when investigating the soil CO_2 degassing rate. Our results also indicate that seismic activity can generate new migration pathways beyond faults which enhance surface emission of CO_2. These factors have an important impact on the total CO_2 output calculated, as there would be great changes in the degassing areas.

Due to the various degassing conditions and different geological backgrounds, it is difficult to accurately estimate the total amount of geogenic CO_2 without sufficient quantifiable data. However, new insights will constantly emerge as additional measurements of CO_2 flux are conducted. For example, global volcanic CO_2 concentrations have increased substantially since CO_2 was measured and addressed in volcanic lakes (Burton et al., 2013). The output obtained in this study also suggested that CO_2 from soil is a promising candidate for global CO_2 emissions. Given that ~38 $Mt.\cdot yr^{-1}$ is produced within a small but seismic area, it is highly possible that the global amount of CO_2 degassing is significantly higher than the current estimated quantity, which is necessary to understand in future investigations.

CRediT authorship contribution statement

Le Hu: Writing – original draft, Investigation, Conceptualization. **Ying Li:** Writing – review & editing, Validation, Funding acquisition. **Zhaofei Liu:** Software, Investigation, Data curation. **Chang Lu:** Visualization, Investigation, Formal analysis. **Giovanni Martinelli:** Writing – review & editing, Validation, Conceptualization. **Galip Yuce:** Methodology, Formal analysis. **Jianguo Du:** Visualization, Validation, Methodology, Formal analysis.

Declaration of competing interest

The authors declare that they have no known competing financial interests or personal relationships that could have appeared to influence the work reported in this paper.

Acknowledgement

This research was supported by the Special Fund from the IEF (CEAIEF20230205, 2024030204), the National Natural Science Foundation of China (60214202), and the IGCP-724 project.

Appendix A. Supplementary data

Supplementary data to this article can be found online at https://doi.org/10.1016/j.gloplacha.2025.104778.

Data availability

The earthquake data were obtained from the China Earthquake Networks Center and National Earthquake Data Center (https://data.earthquake.cn/). The data on the CO_2 flux, altitude, air temperature and soil temperature can be found in Mendeley Data, V1 (https://doi.org/10.17632/cc24zcms6n.1).

References

Allen, M.B., Macdonald, D.I.M., Zhao, X., Vincent, S.J., Brouet-Menzies, C., 1997. Early Cenozoic two-phase extension and late Cenozoic thermal subsidence and inversion of the Bohai Basin, northern China. Mar. Pet. Geol. 14 (7/8), 951–972.

Anderson, T.R., Hawkins, E., Jones, P.D., 2016. CO_2, the greenhouse effect and global warming: from the pioneering work of Arrhenius and Callendar to today's Earth System Models. Endeavour 40 (3), 178–187.

Bond, C.E., Kremer, Y., Johnson, G., Hicks, N., Lister, R., Jones, D.G., Haszeldine, R.S., Saunders, I., Gilfillan, S.M.V., Shipton, Z.K., 2017. The physical characteristics of a CO_2 seeping fault, the implications of fracture permeability for carbon capture and storage integrity. Int. J. Greenh. Gas Con. 61, 49–60.

Bornemann, T.L.V., Adam, P.S., Turzynski, V., Schreiber, U., Figueroa-Gonzalez, P.A., Rahlff, J., Köster, D., Schmidt, T.C., Schunk, R., Krauthausen, B., Probst, A.J., 2022. Genetic diversity in terrestrial subsurface ecosystems impacted by geological degassing. Nat. Commun. 13 (1), 284.

Brune, Sascha, Williams, Simon E., Müller, R., Dietmar., 2017. Potential links between continental rifting, CO_2 degassing and climate change through time. Nat. Geosci. 10 (12), 941–946.

Buono, G., Caliro, S., Paonita, A., Pappalardo, L., Chiodini, G., 2023. Discriminating carbon dioxide sources during volcanic unrest, the case of Campi Flegrei caldera (Italy). Geology 51, 397–401.

Burton, M.R., Sawyer, G.M., Granieri, D., 2013. Deep carbon emissions from volcanoes. Rev. Mineral. Geochem. 75, 323–354.

Buttitta, D., Capasso, G., Paternoster, M., Barberio, M.D., Gori, F., Petitta, Picozzi, M., Petitta, M., Caracausi, A., 2023. Regulation of deep carbon degassing by gas-rock-water interactions in a seismic region of Southern Italy. Sci. Total Environ. 897, 165367.

Cai, J., Chen, X., Dong, Z., Zhan, Y., Liu, Z., Cui, T., Jiang, F., 2023. Three-dimensional electrical structure beneath the epicenter zone and seismogenic setting of the 1976 Ms7.8 Tangshan earthquake, China. Geophys. Res. Lett. 50, e2022GL102291.

Camarda, M., Gregorio, S.D., Capasso, G., Martino, R.M.R.D., Prano, V., 2019. The monitoring of natural soil CO_2 emissions, issues and perspectives. Earth Sci. Rev. 198, 102928.

Caracausi, A., Sulli, A., 2019. Outgassing of mantle volatiles in compressional tectonic regime away from volcanism, the role of continental delamination. Geochem. Geophys. Geosyst. 20 (4), 2007–2020.

Caracausi, A., Camarda, M., Chiaraluce, L., De Gregorio, S., Favara, R., Pisciotta, F.A., 2023. A novel infrastructure for the continuous monitoring of soil CO_2 emissions, a case study at the Alto Tiberina near Fault Observatory in Italy. Front. Earth Sci. 11, 1172643.

Cardellini, C., Chiodini, G., Frondini, F., Avino, R., Bagnato, E., Caliro, S., et al., 2017. Monitoring diffuse volcanic degassing during volcanic unrests, the case of Campi Flegrei (Italy). Sci. Rep. 7, 6757.

Chen, Z., Li, Y., Liu, Z., Lu, C., Zhao, Y., Wang, J., 2019. Evidence of multiple sources of soil gas in the Tangshan fault zone, North China. Geofluids 2019 (1), 1945450.

Chiarabba, C., Gori, P.D., Valoroso, L., Petita, M., Carminati, E., 2022. Large extensional earthquakes push-up terrific amount of fluids. Sci. Rep. 12, 14597.

Chiodini, G., Cioni, R., Guidi, M., Raco, B., Marini, L., 1998. Soil CO_2 flux measurements in volcanic and geothermal areas. Appl. Geochem. 13, 543–552.

Chiodini, G., Cardellini, C., Amato, A., Boschi, E., Caliro, S., Frondini, F., et al., 2004. Carbon dioxide earth degassing and seismogenesis in central and southern Italy. Geophys. Res. Lett. 31, L07615.

Chiodini, G., Granieri, D., Avino, R., Caliro, S., Costa, A., Minopoli, C., 2010. Non-volcanic CO_2 earth degassing, case of mefite d'ansanto (Southern Apennines), Italy. Geophys. Res. Lett. 37, 2323662.

Chiodini, G., Cardellini, C., Luccio, F.D., Selva, J., Ventura, G., 2020. Correlation between tectonic CO_2 earth degassing and seismicity is revealed by a 10-year record in the Apennines, Italy. Sci. Adv. 6, 2938.

Ciotoli, G., Etiope, G., Guerra, M., Lombardi, S., Duddridge, G.A., Grainger, P., 2005. Migration of gas injected into a fault in low-permeability ground. Q. J. Eng. Geol. Hydrogeol. 38 (3), 305.

Ciotoli, G., Bigi, S., Tartarello, C., Sacco, P., Lombardi, S., Ascione, A., Mazzoli, S., 2014. Soil gas distribution in the main coseismic surface rupture zone of the 1980, M_S=6.9, Irpinia earthquake (southern Italy). J. Geophys. Res. Lett.: Solid Earth 119, 2440–2461.

Farsang, S., Louvel, M., Zhao, C., Mezouar, M., Rosa, A.D., Widmer, R.N., 2021. Deep carbon cycle constrained by carbonate solubility. Nat. Commun. 12, 1–9.

Foley, S.F., Fischer, T.P., 2017. An essential role for continental rifts and lithosphere in the deep carbon cycle. Nat. Geosci. 10, 897–902.

Fu, C., Yang, T., Tsai, M., Lee, L., Liu, T., Walia, V., et al., 2017. Exploring the relationship between soil degassing and seismic activity by continuous radon monitoring in the Longitudinal Valley of eastern Taiwan. Chem. Geol. 469, 163–175.

Girault, F., Adhikari, L.B., France-Lanord, C., Agrinier, P., Koirala, B.P., Bhattarai, M., et al., 2018. Persistent CO_2 emissions and hydrothermal unrest following the 2015 earthquake in Nepal. Nat. Commun. 9, 2956.

Gresse, M., Vandemeulebrouck, J., Byrdina, S., Chiodini, G., Bruno, P.P., 2016. Changes in CO_2 diffuse degassing induced by the passing of seismic waves. J. Volcanol. Geotherm. Res. 320, 12–18.

Gutenberg, B., Richter, C.F., 1956. Magnitude and energy of earthquakes. Ann. Geofis. 9, 1–15.

Hazen, R.M., Schiffries, C.M., 2013. Why deep carbon? Rev. Mineral. Geochem. 75 (1), 1–6.

Hencz, M., Biró, T., Németh, K., Porkoláb, K., Kovács, I.J., Sprániz, T., Cloetingh, S., Szabó, C., Berkesi, M., 2023. Tectonically-determined distribution of monogenetic volcanoes in a compressive tectonic regime: an example from the Pannonian continental back-arc system (Central Europe). J. Volcanol. Geotherm. Res. 444, 107940.

Ingebritsen, S.E., Shelly, D.R., Hsieh, P.A., Clor, L.E., Evans, W.C., 2016. Hydrothermal response to a volcano-tectonic earthquake swarm, Lassen, California. Geophys. Res. Lett. 42, 9223–9230.

Italiano, F., Martinelli, G., Plescia, P., 2015. CO_2 Degassing over seismic areas, the role of mechanochemical production at the study case of central Apennines. Pure Appl. Geophys. 165, 175–194.

Kis, B.M., Ionescu, A., Cardellini, C., Harangi, S., Baciu, C., Caracausi, A., Viveiros, F., 2017. Quantification of carbon dioxide emissions of Ciomadul, the youngest volcano of the Carpathian-Pannonian Region (Eastern-Central Europe, Romania). J. Volcanol. Geotherm. Res. 341, 119–130.

Le Voyer, M., Hauri, E.H., Cottrell, E., Kelley, K.A., Salters, V.J., Langmuir, C.H., Hilton, D.R., Barry, P.H., Füri, E., 2019. Carbon fluxes and primary magma CO_2 contents along the global mid-ocean ridge system. Geochem. Geophys. Geosyst. 20 (3), 1387–1424.

Lee, H., Muirhead, J.D., Fischer, T.P., Ebinger, C.J., Kattenhorn, S.A., Sharp, Z.D., et al., 2016. Massive and prolonged deep carbon associated with continental rifting. Nat. Geosci. 9, 145–149.

Lewicki, J.L., Brantley, S.L., 2000. CO_2 degassing along the San Andreas Fault, Parkfield, California. Geophys. Res. Lett. 27, 5–8.

Li, X.R., Wang, J., Zeng, Z., Dai, Q., 2016. Spatial variations of current tectonic stress field and its relationship to the structure and rheology of lithosphere around the Bohai Sea, North China. J. Asian Earth Sci. 139, 83–94.

Liu, B.J., Qu, G.S., Sun, M.X., Liu, K., Zhao, C.B., Xu, X.W., Feng, S.Y., Kou, K.P., 2011. Crustal structures and tectonics of Tangshan earthquake area, results from deep seismic reflection profiling. Seism. Geol. 33, 901–912 (in Chinese with English abstract).

Liu, Y., Zhuang, J., Jiang, C.S., 2020. Background seismicity before and after the 1976 Ms 7.8 Tangshan earthquake: is its aftershock sequence still continuing? Seismol. Res. Lett. 1–9.

Liu, Z., Chen, Z., Li, Y., Zhao, Z., Hong, S., Hu, L., Ma, L., Lu, C., Zhao, Y., He, H., Su, S., Zhao, Y., Shao, W., Cao, Z., Wang, H., 2024. Shale gas leakage and fault activation: Insight from the 2021 Luxian MS 6.0 earthquake, China. Tectonophysics 891, 230530.

Liu, K., Li, Y., Nan, Y., Liu, B., Wang, W., 2022. Detailed shallow structure of the seismogenic fault of the 1976 M_S 7.8 Tangshan earthquake, China. Front. Earth Sci. 10, 946972.

Lopez, T., Fischer, T.P., Plank, T., Malinverno, A., Rizzo, A.L., Rasmussen, D.J., et al., 2023. Tracking carbon from subduction to outgassing along the Aleutian-Alaska Volcanic Arc. Sci. Adv. 28, eadf3024.

Macpherson, C., Mattey, D., 1994. Carbon isotope variations of CO_2 in Central Lau Basin basalts and ferrobasalts. Earth Planet. Sci. Lett. 121 (3–4), 263–276.

Mason, E., Edmonds, M., Turchyn, A.V., 2017. Remobilization of crustal carbon may dominate volcanic arc emissions. Science 357, 290–294.

Mörner, N.A., Etiope, G., 2002. Carbon degassing from the lithosphere. Glob. Planet. Chang. 33, 185–203.

Parks, M.M., Caliro, S., Chiodini, G., Pyle, D.M., Mather, T.A., Berlo, K., et al., 2013. Distinguishing contributions to diffuse CO_2 emissions in volcanic areas from magmatic degassing and thermal decarbonation using soil gas ^{222}Rn–$\delta^{13}C$ systematics, Application to Santorini volcano, Greece. Earth Planet. Sci. Lett. 377, 180–190.

Plank, T., Manning, C.E., 2019. Subducting carbon. Nature 574, 343–352.

Raich, J.W., Schlesinger, W.H., 1992. The global carbon dioxide flux in soil respiration and its relationship to vegetation and climate. Tellus 44B, 81–99.

Raich, J.W., Tufekcioglu, A., 2000. Vegetation and soil respiration, Correlations and controls. Biogeochemistry 48, 71–90.

Sano, Y., Wakita, H., 1985. Geographical distribution of $^3He/^4He$ ratios in Japan: Implications for arc tectonics and incipient magmatism. J Geophys Res 90 (B10), 8729–8741.

Schneider, S.H., 1989. The greenhouse effect: science and policy. Science 243 (4892), 771–781.

Seward, T.M., Kerrick, D.M., 1996. Hydrothermal CO_2 emission from the Taupo Volcanic Zone, New Zealand. Earth Planet. Sci. Lett. 139, 105–113.

Tamburello, G., Pondrelli, S., Chiodini, G., Rouwet, D., 2018. Global-scale control of extensional tectonics on CO_2 earth degassing. Nat. Commun. 9, 4608.

Violay, M., Nielsen, S., Spagnuolo, E., Spagnuolo, E., Cinti, D., Di Toro, G., et al., 2013. Pore fluid in experimental calcite-bearing faults, abrupt weakening and geochemical signature of co-seismic processes. Earth Planet. Sci. Lett. 361, 74–84.

Wang, M., Shen, Z.K., 2020. Present-day crustal deformation of continental China derived from GPS and its tectonic implications. J. Geophys. Res. Solid Earth 125 (2), e2019JB018774.

Wang, X., Li, Y., Du, J., Chen, Z., Zhou, X., Li, X., Cui, Y., Wang, H., Zhang, Z., 2017. Geochemical characteristics of soil gases Rn, Hg and CO, and their genesis in the capital area of China. Acta Seismol. Sin. 39 (1), 85101 (In Chinese with English Abstract).

Wang, Y.C., Zhou, X.C., Tian, J., Zhou, J.L., He, M., Li, J.C., et al., 2023. Volatile characteristics and fluxes of He-CO_2 systematics in the southeastern Tibetan Plateau, Constraints on regional seismic activities. J. Hydrol. 617, 129042.

Yang, Z., Zhang, N., Dong, J., Xia, W., Bao, Z., 2013. Carbon oxygen isotope analysis and its significance of carbonate in the Zhaogezhuang section of early Ordovician in Tangshan, North China. J. Earth Sci. 24, 918–934.

Yuce, G., Fu, C., D'Alessandro, W., Gulbay, A., Lai, C., Bellomo, S., et al., 2017. Geochemical characteristics of soil radon and carbon dioxide within the Dead Sea Fault and Karasu Fault in the Amik Basin (Hatay), Turkey. Chem. Geol. 469, 129–146.

Zhang, M.L., Zhang, L.H., Zhao, W.B., Guo, Z.F., Xu, S., Sano, Y., et al., 2021. Metamorphic CO_2 emissions from the southern Yadong-Gulu rift, Tibetan Plateau, Insights into deep carbon cycle in the India-Asia continental collision zone. Chem. Geol. 584, 120534.

Zhang, G.W., Ji, Y., Guo, H., Hu, X.P., 2022. Complex fault geometry of the 1976 M_S 7.8 Tangshan earthquake source region in North China. Tectonophysics 845, 229642.

Zhao, W.B., Guo, Z.F., Sun, Y.T., Zhang, M.L., Zhang, H.L., Lei, M., et al., 2018. Advances of the research on CO_2 degassing from volcanic fields. Bull. Mineral. Petrol. Geochem. 37, 601–620 (in Chinese with English abstract).